analytical chemistry

pubs.acs.org/ac Article

Clinical-Scale Production of Nearly Pure (>98.5%) Parahydrogen and Quantification by Benchtop NMR Spectroscopy

Shiraz Nantogma,[‖] Baptiste Joalland,[‖] Ken Wilkens, and Eduard Y. Chekmenev*

Cite This: *Anal. Chem.* 2021, 93, 3594−3601 Read Online

ACCESS | Metrics & More | Article Recommendations | Supporting Information

ABSTRACT: Because of the extensive chemical, physical, and biomedical applications of parahydrogen, the need exists for the development of highly enriched parahydrogen in a robust and efficient manner. Herein, we present a parahydrogen enrichment equipment which substantially improves upon the previous generators with its ability to enrich parahydrogen to >98.5% and a production rate of up to 4 standard liters per minute with the added advantage of real-time quantification. Our generator employs a pulsed injection system with a 3/16 in. outside diameter copper spiral tubing filled with iron-oxide catalyst. This tubing is mated to a custom-made copper attachment to provide efficient thermal coupling to the cold head. This device allows for robust operation at high pressures up to 34 atm. Real-time quantification by benchtop NMR spectroscopy is made possible by direct coupling of the *p*-H_2 outlet from the generator to a 1.4 T NMR spectrometer using a regular 5 mm NMR tube that is continuously refilled with the exiting parahydrogen gas at ∼8 atm pressure. The use of high hydrogen gas pressure offers two critical NMR signal detection benefits: increased concentration and line narrowing. Our work presents a comprehensive description of the apparatus for a convenient and robust parahydrogen production, distribution, and quantification system, especially for parahydrogen-based hyperpolarization NMR research.

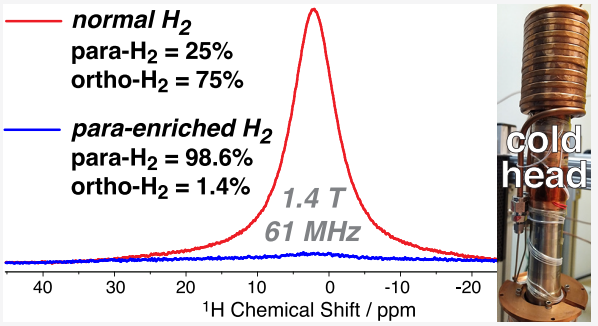

The sensitivity of nuclear magnetic resonance techniques is limited by low spin polarization *P* at clinically relevant conditions. One way to mitigate this limitation and increase *P* is to utilize NMR hyperpolarization, where nuclear spin polarization is artificially and temporarily created. Currently, there are three leading hyperpolarization methods:[1−3] spin exchange optical pumping (SEOP),[4] dissolution dynamic nuclear polarization (d-DNP),[5] and parahydrogen-induced nuclear polarization (PHIP).[6,7] The first two techniques require the use of very powerful, sophisticated, and expensive equipment together with very long turnover times to produce hyperpolarized (HP) compounds.[8,9] These techniques have advanced to clinical studies.[10,11] A higher throughput and less expensive hyperpolarization alternative is PHIP, which exploits the spin order of parahydrogen (*p*-H_2) singlet to induce nuclear spin polarization.[12,13] This can be accomplished either through hydrogenative PHIP[2,6,7] or via its non-hydrogenative variant signal amplification by reversible exchange (SABRE).[14−16] The latter relies on the simultaneous chemical exchange of *p*-H_2 and a to-be-hyperpolarized substrate on a hexacoordinate metal complex.[14] When the nuclear spin level anticrossings[17] are established, the polarization is spontaneously transferred from *p*-H_2-derived hydrides to the target nucleus of the substrate.[18] In the case of PHIP, the polarization of the nascent *p*-H_2-derived protons in PHIP can be transferred to heteronuclei via magnetic field cycling or through the use of specially designed radio frequency (RF) pulse sequences.[19−25]

Recently, parahydrogen-hyperpolarized compounds have attracted special interest for various applications in both catalysis (reaction progress monitoring) and in biomedicine as MRI contrast agents.[1,12] Examples include HP ^{13}C-succinate to image brain cancer cells of rats *ex vivo*[26] and HP ^{13}C-pyruvate to detect metabolic dysfunction in cardiomyopathy via real-time *in vivo* mapping of HP ^{13}C-pyruvate and ^{13}C-lactate.[27] Proton-hyperpolarized propane gas is another example for prospective use in subsecond pulmonary functional MRI.[28,29] A detailed review on bio-imaging PHIP technology can be found elsewhere.[12] Yet, despite these far-reaching applications of *p*-H_2, its enrichment to very high levels and quantification and distribution in a comprehensive manner is still a translational challenge. Therefore, there is a need to find faster, easier, efficient, and more comprehensive ways to produce and quantify *p*-H_2 in the context of biomedical applications.

Received: December 8, 2020
Accepted: January 22, 2021
Published: February 4, 2021

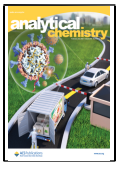

https://dx.doi.org/10.1021/acs.analchem.0c05129
Anal. Chem. 2021, 93, 3594−3601

The conventional route to enrich p-H_2 mixture is to shift the equilibrium state of molecular dihydrogen, which exists predominantly in the ortho-/para-state in a 3:1 ratio, toward the para-state by cryogenic cooling to very low temperatures in the presence of a suitable catalyst to accelerate the otherwise forbidden (and thus slow) transition. Up to 50% enrichment is obtained with liquid nitrogen temperature as the cooling source and activated charcoal as the catalyst.[30] Other materials were employed as hydrogen spin conversion catalysts.[31,32] Moreover, enrichment of up to 99.99% is possible with specialized cryogenic equipment, which can reduce the catalyst temperature down to 10 K.[33] For example, Hövener and co-workers have designed a continuous-flow high-throughput [4 standard liters per minute (SLM)] generator suitable for clinical settings with p-H_2 enrichment of up to 98%.[34] Prior to that, we had reported a pulsed injection method to produce up to 98% p-H_2 at a rate of 0.9 SLM.[35] The advantage of the pulsed injection method is that it provides a rather simple way to control the contact time of orthohydrogen with the catalyst without the use of specialized equipment such as a mass-flow controller.[36] However, these two previous designs employed a rather large copper chamber filled with catalyst. In our experience, this chamber covered with a copper lid with indium metal seal is highly susceptible to wear over multiple cryogenic cycles—as a result, the seal leaks, resulting in significantly reduced operating pressure.

Production of p-H_2 using liquid N_2 as a cooling source (*ca.* 77 K at 1 atm) is the least expensive and the least complex gateway to PHIP and SABRE hyperpolarization techniques. Such a generator can be constructed fairly easily or obtained commercially (*ca.* 3300 EURO, XeUS Technologies, LTD, Nicosia, Cyprus). Parahydrogen spin conversion at 77 K yields approximately 49−50% p-H_2. Indeed, a number of hyperpolarization studies have been reported using such designs.[37−40] However, it should be made abundantly clear that HP signal is reduced by a factor of 3.0 when using 50% p-H_2 as compared to near 100% p-H_2.[12,37] While this 3-fold reduction may not be an impediment for the majority of HP NMR studies, the 3-fold boost is highly advantageous when the signal-to-noise ratio (SNR) is limited. Examples of such cases include working with natural-abundance ^{13}C- and ^{15}N-compounds or *in vivo* applications.[37,41−46]

To mitigate the previous design shortcomings, we present a portable high-throughput p-H_2 generator design, which builds on the work of Feng et al.[35] and Tom et al.[47] Our new substantially improved design employs a spiral copper tubing filled with catalyst, which operates at high pressures of up to 34 atm. We demonstrate p-H_2 production at rates up to 4 SLM with enrichment levels greater than 98.5%. This flow rate represents a more than 4-fold improvement of Feng et al.'s[35] design and a 6-fold improvement of Tom et al.[47] and other similar designs, which demonstrated production of more than 98% p-H_2.[32,48,49] The air-cooled system employed in our device is stand-alone and semi-automated—this means that the device can be sited without the requirement of a water chilling source. Moreover, we demonstrate that the p-H_2 fraction can be conveniently quantified using a benchtop NMR spectrometer allowing for near real-time monitoring of p-H_2 production. The described p-H_2 quantification is compared to a more established high-field detection with the advantages of being substantially lower cost, more convenient, less time consuming, and very useful in longitudinal studies. The reported device has been successfully employed for a wide range of experiments employing p-H_2 as a source of NMR hyperpolarization. Here, we also provide two illustrative utility examples of our generator to enhance nuclear spin polarization via hydrogenative and non-hydrogenative PHIP.

MATERIALS AND METHODS

The overall generator schematic is shown in Figure 1 and the annotated photograph is provided in Figure 2. The catalyst-

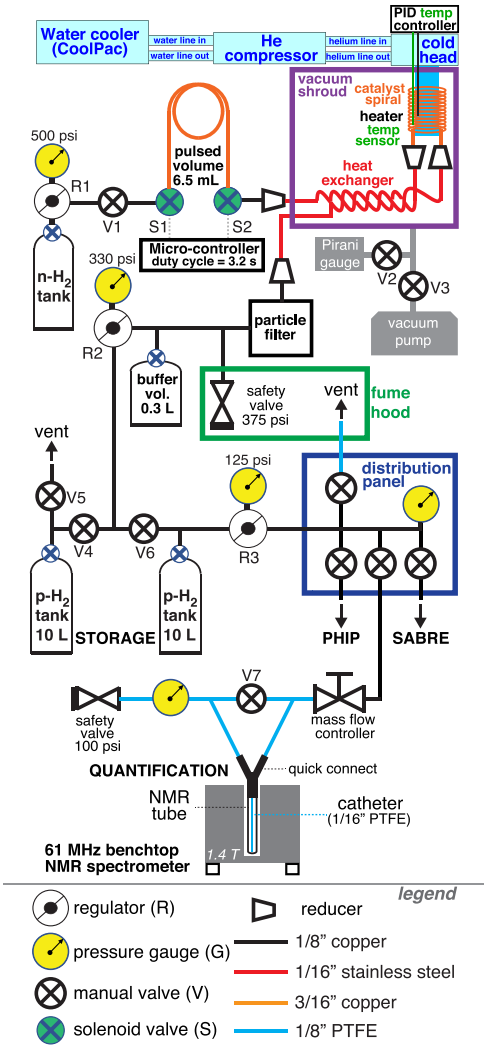

Figure 1. Schematic diagram of the parahydrogen generator. R = pressure regular; G = pressure gauge; V = manual valve; S = solenoid valve. The adapters employed are made of stainless steel for compression tubing. All tees employed with copper tubing are made of brass; V4, V5, V6 are brass ball valves.

filled copper tubing [3/16 in. (″) outer diameter (OD), 0.128″ inner diameter cleaned copper tubing, McMaster Carr 5174K2] spiral coil is made of nine turns to pack approximately 5−10 g of paramagnetic hydrated iron(III) oxide ($Fe_2O_3 \cdot H_2O$, 371254, Sigma-Aldrich, St. Louis, MO)—see the Supporting Information for details. The catalyst was washed with ethanol to eliminate microparticles. This copper tubing is tightly fitted into the helical copper core attached to a cold head to enable efficient heat transfer (Figures 3 and S1). The copper cylinder with machined hollow helical grooves was custom designed such that each winding of the copper coil tubing fits tightly into the equally spaced grooves for good

https://dx.doi.org/10.1021/acs.analchem.0c05129
Anal. Chem. 2021, 93, 3594−3601

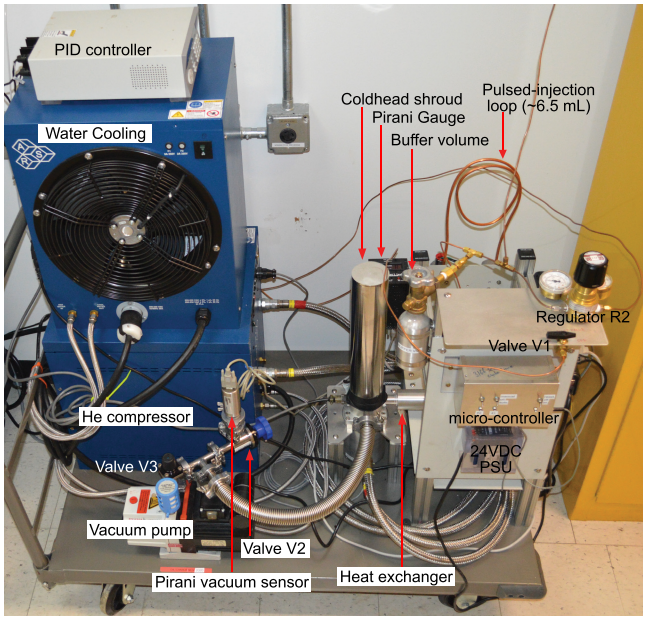

Figure 2. Annotated view of the essential components of the generator manifold without the storage tanks. These major components are connected to each other through copper and stainless-steel tubing. See the Supporting Information for more details.

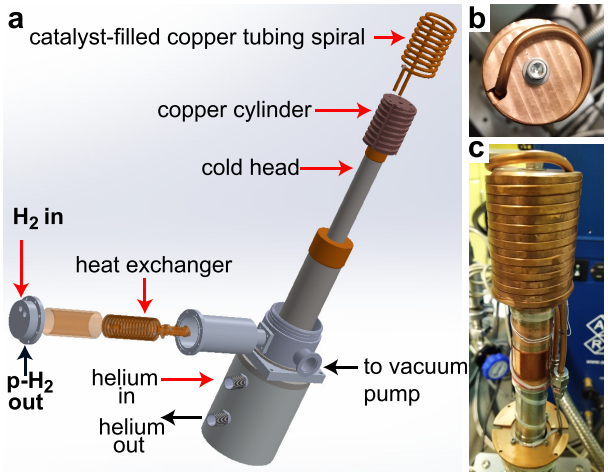

Figure 3. (a) Annotated 3D rendering of cold head assembly. (b) Top view of catalyst chamber with the top winding running along the length of copper core. (c) Side view of catalyst chamber sitting on the cold head. The tubing employed in the heat exchanger is made of stainless steel. See the Supporting Information for more details.

thermal contact between the copper spiral and the copper cylinder attached to the cold head, Figure 3. The copper cylinder mounts to the cold head using a stainless steel bolt (Figure 3b). Commercially available water-cooled helium compressor [ARS-4HW, Advances Research Systems (ARS), Macungie, PA] provides a cooling source to a cold head (model DE-204, ARS, Macungie, PA). An air-cooled cooling module (model CoolPac, ARS, Macungie, PA) provides a cooling source to the helium compressor with both devices operating using 240 VAC.

The CoolPac eliminates the need for external water cooling by recirculating water with the helium compressor. A particle filter (1/8″ Tube OD, rated to 3000 psi, Brass Housing, McMaster Carr 9816K71) is connected to the exit line of the catalyst chamber to capture catalyst microparticles to prevent their passage to the storage tanks. A 0.3 L aluminum tank (M2, Catalina Cylinders, Garden Grove, CA, USA) is employed as temporary storage (buffer volume) with a 350−500 psi rated safety valve venting to the fume hood, Figure 1. Brass manual valves (miniature ball valves by Parker) and brass regulators are situated at various points along the generator lines to provide control and safety of hydrogen gas flow. The cold head assembly is operated under vacuum by connecting it to a vacuum pump (Duo 2.5 Rotary Vane Vacuum Pump, Pfeifer, PKD41602A) and Pirani vacuum gauge via V3 and V2 valves, respectively (Figure 1).

During operation, the normal ultrahigh purity (>99.999%) hydrogen gas is directed from the storage tank via high-pressure solenoid valves S1 and S2 (Series 20, 2-way NC, Peter Paul Electronics, New Britain, CT) to the rest of the generator manifold. These solenoid valves are controlled by an open-source Arduino microcontroller programmed to operate with a duty cycle of 3.2 s. Stainless steel adapters (Swagelok) for compression tubing were used to change the sizes and types of tubing at various stages of the generator.

RESULTS AND DISCUSSION

Mode of Operation. There are three phases in the p-H_2 enrichment process of the generator operation cycle: the generator cooling, p-H_2 conversion, and p-H_2 production phases. The first phase is the cooling phase, and to begin, the chamber surrounding the cold head must be evacuated (to minimize thermal losses), which is performed by turning on the vacuum pump and then opening valve V3 (Figure 1). Once the evacuation process starts, the main gas flow line is pressurized to approximately 460 psi using the regulator R1 followed by the opening of inlet valve V1. The pulsed injection is then switched on using the Arduino microcontroller to start the H_2 flow at ∼4 SLM. This approach ensures that there is H_2 gas flow during the cooling process to purge any condensed contaminants that might have been deposited during the previous production cycle.

Generator Cooling. During the cooling phase, the hydrogen gas is vented through the safety valve. The vacuum around the cold head around the catalyst chamber is monitored by a Pirani 945 controller with a series 345 vacuum gauge (Kurt J. Lesker, Pittsburgh, PA). When the pressure reaches the range of $(2-4) \times 10^{-2}$ mbar, the helium DE-204 compressor and CoolPac (water cooler) are turned on. Once the compressor is running, the temperature controller is switched on together with the proportional−integral−derivative temperature controller, and the temperature is set at the desired point (e.g., 27 K). The generator is left on afterward for approximately 2 h and allowed to chill the catalyst chamber to the set temperature.

Parahydrogen Conversion. Parahydrogen conversion is the second phase of the p-H_2 enrichment process, which starts in the catalyst spiral once the desired set point is reached. Normal hydrogen is delivered to the catalyst chamber at high pressure (≥460 psi overpressure) in a pulsed cycle of 3.2 s. At the beginning of the cycle, the production rate is the highest (∼4 SLM) because of the large pressure gradient between the source (460 psi overpressure) and the storage tank (0 psi overpressure). The production rate is the slowest at the end of the production cycle (*ca.* 330 psi final pressure in storage tanks): 1.4 SLM. The production rate can be adjusted via

https://dx.doi.org/10.1021/acs.analchem.0c05129
Anal. Chem. 2021, 93, 3594−3601

reprogramming the cycle time of the microcontroller or varying the volume of the copper tubing between solenoid valves S1 and S2 (currently set to ∼6.5 mL). Because hydrogen has a high heat capacity, formation of frost has been observed in previous generators[35] along the exit line due to atmospheric moisture condensation on the cold exit tubing. Formation of frost is the sign of substantial cooling of the outer parts of the device—this is a potential problem because the vacuum chamber surrounding the cold head may lose vacuum due to partial loss of the sealing due to shrinking O-ring seals—the partial loss in vacuum ultimately leads to operational temperatures well above the desired ≤27 K and correspondingly lower p-H_2 fraction. Moreover, if the moisture accumulates inside the vacuum shroud (Figure 1), a substantial downtime will be required to dry out the device. Our generator solves this shortcoming by passing the cold enriched p-H_2 through a heat exchanging system to establish thermal equilibrium between the entering (room temperature) normal H_2 and the exiting (cryogenic temperature) p-H_2. The heat exchanger is made of two 1/16″ stainless-steel tubes tightly coiled around each other in a helix, where one of them leads into the catalyst chamber and the other is the outlet. Consequently, cold p-H_2 and warm hydrogen give out negative and positive heat, respectively, when they pass over each other and a freeze out of the line is avoided.

Parahydrogen Collection. Parahydrogen collection is the last phase of the production process. After p-H_2 passes through the heat exchanger, it travels through the particle filter to remove any residual and unwanted particles that may be found in the exiting p-H_2 gas. An adapter stationed before the particle filter conveniently changes the tubing from stainless steel to copper. The temporary (buffer) storage is added to buffer the pressure jumps of the pulsed operation. It is important to note that the temporary storage tank is connected through a long tube to a safety valve rated 350−500 psi (tuned to 375 psi), which is placed in the fume hood. Overall, this prevents operation of the pressurized line above 375 psi. When the pressure inside the temporary storage is sufficiently high (and the temperature of the catalyst is low, e.g., 27K), which can be monitored using regulator R2, the manual valves V4 and V6 together with the tank valves are opened and p-H_2 flows into the final storage tanks. The tanks can be filled one at a time or filled simultaneously by opening both valves. Other arrangements of the storage tank filling process can be envisioned too. Alternatively, both tanks can be closed and the p-H_2 gas bypasses the distribution panel for either p-H_2 experiments or quantification. One crucial factor to note is that these storage tanks are made of aluminum to minimize wall relaxation. From these storage tanks, we feed p-H_2 through a custom-built distribution panel (built with copper tubing and brass Swagelok fittings and Swagelok or Parker brass ball valves) to appropriate containers for various PHIP and SABRE experiments.

Parahydrogen Quantification. Parahydrogen quantification by NMR spectroscopy is not straightaway since p-H_2 is NMR inactive. Several methods have been devised such as the use of Raman spectroscopy to measure the first two rotational bands of the spin isomers of normal H_2.[50] Matrix isolation spectroscopy, thermal conductivity, relaxation kinetics in borosilicate glass, and other para-/ortho-quantification methods exist too.[33,35,51] We utilized the indirect approach to quantify the level of enrichment by measuring the NMR signal of residual orthohydrogen using conventional high-field 9.4 T NMR spectroscopy and also "real-time" monitoring of the exiting p-H_2 using bench-top 1.4 T NMR spectrometer. The spectrum obtained at 9.4 T after enrichment was compared to that of normal hydrogen to calculate the degree of enrichment. Figure 4b shows the spectra for both normal hydrogen and

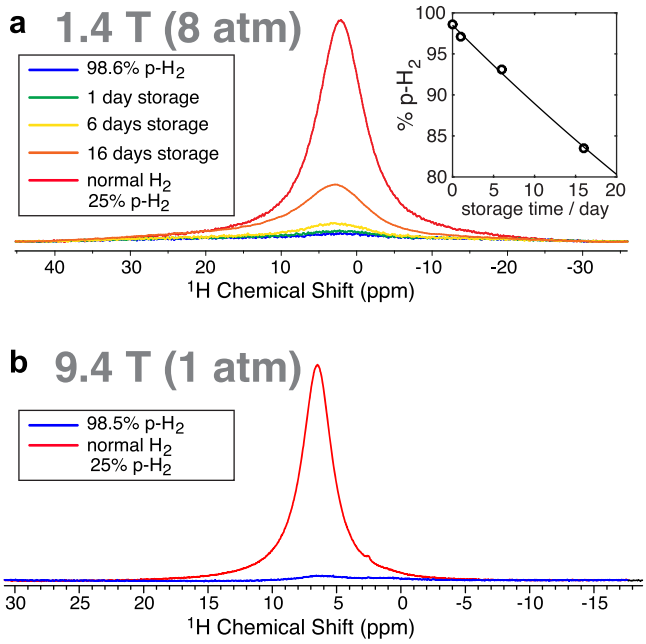

Figure 4. (a) Parahydrogen quantification using 1.4 T NMR spectrometer operating at 61 MHz proton resonance frequency using gas samples at 8 atm. Acquisition parameters: 1024 scans, 5 kHz spectral width, 52 ms acquisition time, 0.1 s repetition time, ∼102 s total acquisition time, 90° excitation pulse. The inset display shows the decay of p-H_2 in the aluminum storage tank. (b) Parahydrogen quantification using 9.4 T Varian NMR spectrometer operating at 400 MHz proton resonance frequency using gas samples at 1 atm. Acquisition parameters: 512 scans, 20 kHz spectral width, 52 ms acquisition time, 0.1 s repetition time, ∼52 s total acquisition time, 90° excitation pulse.

para-enriched hydrogen from the generator at 1 SLM_{MAX} production rate. Using eq 1, the p-H_2 percentage was calculated to be ≥ 98.5% for 1 and 4 SLM_{MAX} production rates.

However, it is important to note that in order to do high-field quantification, the NMR tube had to be carefully filled and quickly transported to the NMR spectrometer (Varian) to avoid significant relaxation due to contact with the NMR tube glass walls and other environmental variables (e.g., residual O_2). Thus, we demonstrate a more convenient and efficient approach to quantify the level of enrichment in real-time to avoid losses due to glass-wall relaxations and to save overall quantification time. Hence, we interfaced the outlet of the p-H_2 generator to an NMR tube via a Teflon tube with a mass flow controller (MFC) and pressure regulator setup described previously.[22] This setup enables direct quantification of p-H_2 as it exits the generator using a 1.4 T benchtop NMR spectrometer (Spinsolve ^{13}C, Magritek, New Zealand) and eliminates the need for inconvenient and time-consuming NMR tube filling and transportation for quantification. Additionally, since low-field benchtop NMR spectrometers are becoming a more common commodity and many PHIP experiments are performed with them, using them for real-time quantification offers an additional benefit. Specifically, p-H_2

https://dx.doi.org/10.1021/acs.analchem.0c05129
Anal. Chem. 2021, 93, 3594−3601

produced is typically employed in the 5 mm NMR tube for p-H_2 bubbling experiments using PHIP or SABRE. The p-H_2 quantification is therefore performed at the point of p-H_2 utilization after it has passed through gas lines (including MFC made of stainless steel) and enters the empty 5 mm NMR tube that will be employed for the future PHIP or SABRE experiments. Here, we operate our setup at a 100 psi overpressure in economy 5 mm NMR tubes (WG-1000-8, Wilmad glass) to quantify the level of para-enrichment. It was found to be 98.6%, which is in good agreement with the value obtained using a 9.4 T NMR spectrometer. Operating at high pressure offers two critical advantages in the context of low-field detection, which is typically SNR challenged. First, the NMR line is decreased in units of Hz from ∼1.2 kHz at 1 atm (Figure 4b) to 0.6 kHz at ∼8 atm (Figure 4a). Second, the higher gas-phase concentration boosts the NMR signal by ∼8-fold. As a result, the cumulative SNR benefit of this high-pressure approach is a factor of ∼16 corresponding to a factor of ∼256 in time-saving. Therefore, it becomes possible to perform p-H_2 quantification at 1.4 T with a total scan time of less than 2 min. We anticipate that lower field NMR spectrometers can also be successfully employed for the purpose of p-H_2 quantification using eq 1

$$f = 1 - \frac{3(\text{enriched signal})}{4(\text{unenriched signal})} \quad (1)$$

where f is the p-H_2 fraction. Note that the multipliers 3 and 4 are used to reflect the presence of 1/4 (25%) of p-H_2 in normal (unenriched) dihydrogen gas.[12] Furthermore, the p-H_2 decay curve of p-H_2 stored in an aluminum tank obtained for four data points for 16 days using a 1.4 T device showed that the percentage of enriched p-H_2 decreased by only ∼15% by the 16th day. In practical terms, this storage system enables our lab with potent p-H_2 within 2−3 weeks after the production process.

Generator Utility for Parahydrogen-Induced Polarization Experiments. Generator utility for parahydrogen-induced polarization experiments was demonstrated in a wide range of PHIP and SABRE studies since the commencement of this device in March 2019.[22,52−57]

To demonstrate the utility of ^{15}N hyperpolarization in microtesla magnetic field using SABRE in SHield Enables Alignment Transfer to Heteronuclei (SABRE-SHEATH)[58] technique (Figure 5a) with the presented p-H_2 generator, we used 2 mM of Ir(COD)(IMes)Cl [IMes = 1,3-bis(2,4,6-trimethylphenyl)imidazol-2-ylidene; COD = cycloocta-diene][59,60] as a precatalyst and 20 mM each of the substrates (isotopologues of metronidazole enriched with ^{15}N at two positions or all three nitrogen sites, Figure 5c,d). Each substrate sample was hyperpolarized in a magnetic shield operating in the microtesla regime and then transferred afterward to an NMR spectrometer for measurements. The HP signal was referenced against neat thermally polarized pyridine-^{15}N, Figure 5b. The polarization was performed by bubbling p-H_2 into an NMR tube containing the substrate and the activated polarization transfer catalyst for 50−100 s in CD_3OD. For metronidazole-$^{15}N_3$ (Figure 5d), where all nitrogen sites are ^{15}N-labeled, ^{15}N polarization values were up to ∼16%.[52] The ^{15}N P values were drastically decreased in metronidazole-$^{15}N_2$ (Figure 5c) yielding ^{15}N polarization values of up to 4% in otherwise identical conditions due to less favorable relaxation dynamics in microtesla magnetic field

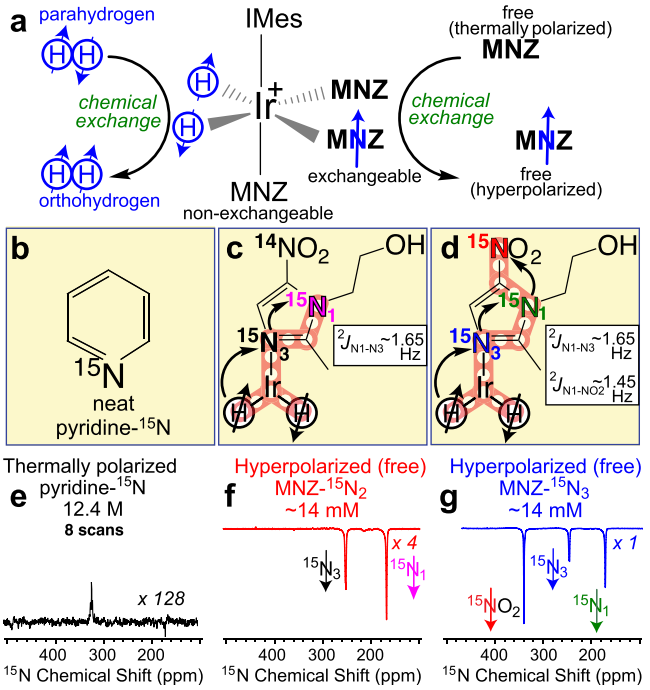

Figure 5. (a) Molecular exchange between p-H_2 and metronidazole leading to SABRE hyperpolarization. (b) Neat pyridine-^{15}N was employed as a signal reference. (c,d) Structures and polarization transfer via spin-relay between p-H_2 and ^{15}N nuclei in ^{15}N-isotopologues of metronidazole. (e) Reference ^{15}N NMR spectrum of a thermally polarized neat pyridine-^{15}N acquired with eight scans and a recovery time of 10 min. (f,g) Single-scan ^{15}N NMR spectra of SABRE-hyperpolarized metronidazole-$^{15}N_2$ and metronidazole-$^{15}N_3$. Reproduced from ref 52 with permission from The Royal Society of Chemistry.

because of the presence of ^{14}N spin in metronidazole-$^{15}N_2$.[52] This finding is important as it guides more rational design of ^{15}N-hyperpolarized contrast agents and nitro-imidazole-based drugs for future molecular imaging of hypoxia and more advanced theragnostic applications.[52,54]

Last, we demonstrate the utility of the p-H_2 generator reported here for creating of parahydrogen-induced radio amplification by stimulated emission of radiation (PHIP-RASER) effect.[53,55,61] Parahydrogen was bubbled for 10 s into a solution containing ∼200 mM ethyl vinyl substrate and 4 mM Rh-based hydrogenation catalyst in CD_3OD at Earth's magnetic field (Figure 6a).[53] This experiment resulted in a proton polarization of 8.4% (reference signal of thermally polarized ethyl 1-^{13}C-acetate (EA-1-^{13}C), Figure 6c,b. Spontaneous occurrence of PHIP-RASER in a 61 MHz benchtop NMR spectrometer is shown in Figure 6d.[53] These results are important because they demonstrate that PHIP can be conveniently employed to generate the RASER effect in standard NMR equipment.

CONCLUSIONS

In conclusion, we have presented a home-built pulse-injection p-H_2 generator employing a copper tubing spiral filled with catalyst. We estimate the cost of the components utilized on the order of 55,000 USD *ca.* 2020. In addition, we expect that it would require approximately 4−6 months of PhD- or MS-skilled person to assemble the described equipment, make custom components, and to perform quality assurance. The

https://dx.doi.org/10.1021/acs.analchem.0c05129
Anal. Chem. 2021, 93, 3594−3601

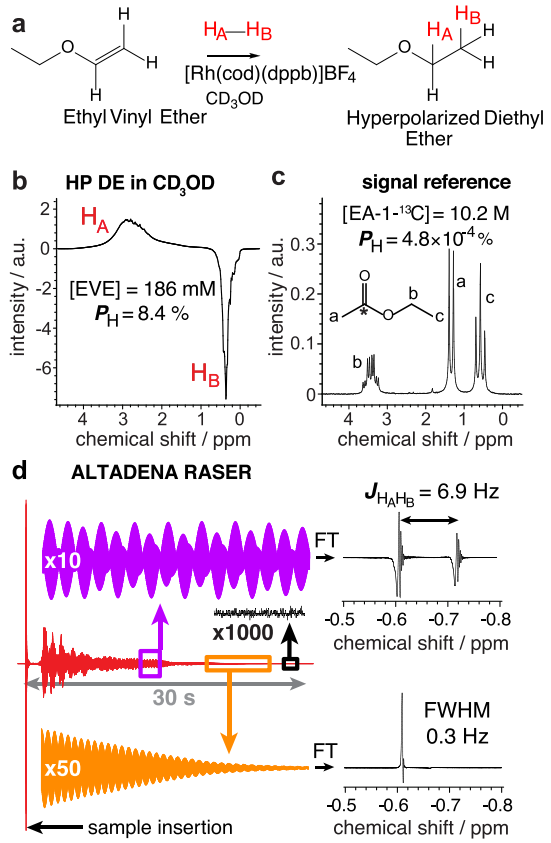

Figure 6. (a) Reaction of ethyl vinyl ether with p-H_2 (shown as H_A–H_B) in CD_3OD in the presence of Rh-based catalyst resulting in the production of HP diethyl ether (DE).[53] (b) NMR spectrum of HP protons of DE, $P_H \sim 8.4\%$. (c) NMR spectrum of thermally polarized EA-1-^{13}C as a signal reference for polarization and chemical shift comparisons. (d) FID and Fourier transformed spectra of HP DE with a resonance width of 0.3 Hz and a J-coupling of HP protons at 6.9 Hz. Acquisition parameters: NMR tube inserted 2–3 s after initiating the pulse acquisition sequence in the 61 MHz benchtop NMR spectrometer, with a pulse angle <0.1° and an opened ^{1}H detector channel for 32 s. Reprinted with permission from ref 53.

generator is portable enough to be easily transported within a building or in a vehicle. Maximum enrichment of >98.5% was achieved at a pressure of 375 psi and a set temperature of 27 K with a production rate of up to 4 SLM. Further modifications can be carried out to achieve various production targets. For instance, by increasing the size of the tubing volume between the S1 and S2 solenoid valves of the injection manifold, production rates can be further increased. Real-time p-H_2 quantification of the produced p-H_2 gas was demonstrated using a bench-top 1.4 T NMR spectrometer using pressurized exiting (~8 atm) p-H_2 gas in real-time. High production rate and real-time quantification of p-H_2 gas bode well for biomedical translation of parahydrogen-hyperpolarized contrast agents. To that end, the utility of the generator has been successfully demonstrated for the production of several proton- and ^{15}N-hyperpolarized contrast agents. We also envision a wide range of other HP studies that can be enabled by this device ranging from biomedical HP MRI[46,54,62,63] to HP spectroscopy of reaction monitoring.[39]

■ ASSOCIATED CONTENT

Supporting Information

The Supporting Information is available free of charge at https://pubs.acs.org/doi/10.1021/acs.analchem.0c05129.

Additional drawings and photographs of the described equipment and operational manual for the reported device (PDF)

■ AUTHOR INFORMATION

Corresponding Author

Eduard Y. Chekmenev − *Department of Chemistry, Integrative Biosciences (Ibio), Wayne State University, Detroit, Michigan 48202, United States; Russian Academy of Sciences, Moscow 119991, Russia;* orcid.org/0000-0002-8745-8801; Email: chekmenevlab@gmail.com

Authors

Shiraz Nantogma − *Department of Chemistry, Integrative Biosciences (Ibio), Wayne State University, Detroit, Michigan 48202, United States*

Baptiste Joalland − *Department of Chemistry, Integrative Biosciences (Ibio), Wayne State University, Detroit, Michigan 48202, United States;* orcid.org/0000-0003-4116-6122

Ken Wilkens − *Department of Radiology and Radiological Sciences, Vanderbilt University Institute of Imaging Science (VUIIS), Nashville, Tennessee 37232-2310, United States*

Complete contact information is available at: https://pubs.acs.org/10.1021/acs.analchem.0c05129

Author Contributions

‖S.N. and B.J. contributed equally.

Notes

The authors declare the following competing financial interest(s): EYC declares a stake of ownership in XeUS technologies LTD.

■ ACKNOWLEDGMENTS

This work was supported by the National Science Foundation under grants CHE-1904780, by the National Cancer Institute under 1R21CA220137, NHLBI under HL154032-01, and by DOD CDMRP under BRP W81XWH-12-1-0159/BC112431, PRMRP W81XWH-15-1-0271, and W81XWH-20-10576.

■ REFERENCES

(1) Nikolaou, P.; Goodson, B. M.; Chekmenev, E. Y. *Chem.—Eur. J.* **2015**, *21*, 3156–3166.

(2) Goodson, B. M.; Whiting, N.; Coffey, A. M.; Nikolaou, P.; Shi, F.; Gust, B. M.; Gemeinhardt, M. E.; Shchepin, R. V.; Skinner, J. G.; Birchall, J. R.; Barlow, M. J.; Chekmenev, E. Y. *Emagres* **2015**, *4*, 797–810.

(3) Kovtunov, K. V.; Pokochueva, E. V.; Salnikov, O. G.; Cousin, S. F.; Kurzbach, D.; Vuichoud, B.; Jannin, S.; Chekmenev, E. Y.; Goodson, B. M.; Barskiy, D. A.; Koptyug, I. V. *Chem.—Asian J.* **2018**, *13*, 1857–1871.

(4) Walker, T. G.; Happer, W. *Rev. Mod. Phys.* **1997**, *69*, 629–642.

(5) Ardenkjaer-Larsen, J. H.; Fridlund, B.; Gram, A.; Hansson, G.; Hansson, L.; Lerche, M. H.; Servin, R.; Thaning, M.; Golman, K. *Proc. Natl. Acad. Sci. U.S.A.* **2003**, *100*, 10158–10163.

(6) Eisenschmid, T. C.; Kirss, R. U.; Deutsch, P. P.; Hommeltoft, S. I.; Eisenberg, R.; Bargon, J.; Lawler, R. G.; Balch, A. L. *J. Am. Chem. Soc.* **1987**, *109*, 8089–8091.

(7) Bowers, C. R.; Weitekamp, D. P. *Phys. Rev. Lett.* **1986**, *57*, 2645–2648.

(8) Ardenkjaer-Larsen, J. H.; Leach, A. M.; Clarke, N.; Urbahn, J.; Anderson, D.; Skloss, T. W. *NMR Biomed.* **2011**, *24*, 927−932.
(9) Ardenkjaer-Larsen, J. H. *J. Magn. Reson.* **2016**, *264*, 3−12.
(10) Mugler, J. P.; Altes, T. A. *J. Magn. Reson. Imag.* **2013**, *37*, 313−331.
(11) Nelson, S. J.; Kurhanewicz, J.; Vigneron, D. B.; Larson, P. E. Z.; Harzstark, A. L.; Ferrone, M.; van Criekinge, M.; Chang, J. W.; Bok, R.; Park, I.; Reed, G.; Carvajal, L.; Small, E. J.; Munster, P.; Weinberg, V. K.; Ardenkjaer-Larsen, J. H.; Chen, A. P.; Hurd, R. E.; Odegardstuen, L.-I.; Robb, F. J.; Tropp, J.; Murray, J. A. *Sci. Transl. Med.* **2013**, *5*, 198ra108.
(12) Hövener, J.-B.; Pravdivtsev, A. N.; Kidd, B.; Bowers, C. R.; Glöggler, S.; Kovtunov, K. V.; Plaumann, M.; Katz-Brull, R.; Buckenmaier, K.; Jerschow, A.; Reineri, F.; Theis, T.; Shchepin, R. V.; Wagner, S.; Bhattacharya, P.; Zacharias, N. M.; Chekmenev, E. Y. *Angew. Chem., Int. Ed.* **2018**, *57*, 11140−11162.
(13) Green, R. A.; Adams, R. W.; Duckett, S. B.; Mewis, R. E.; Williamson, D. C.; Green, G. G. R. *Prog. Nucl. Magn. Reson. Spectrosc.* **2012**, *67*, 1−48.
(14) Rayner, P. J.; Duckett, S. B. *Angew. Chem., Int. Ed.* **2018**, *57*, 6742−6753.
(15) Adams, R. W.; Aguilar, J. A.; Atkinson, K. D.; Cowley, M. J.; Elliott, P. I. P.; Duckett, S. B.; Green, G. G. R.; Khazal, I. G.; Lopez-Serrano, J.; Williamson, D. C. *Science* **2009**, *323*, 1708−1711.
(16) Adams, R. W.; Duckett, S. B.; Green, R. A.; Williamson, D. C.; Green, G. G. R. *J. Chem. Phys.* **2009**, *131*, 194505.
(17) Pravdivtsev, A. N.; Yurkovskaya, A. V.; Vieth, H.-M.; Ivanov, K. L.; Kaptein, R. *ChemPhysChem* **2013**, *14*, 3327−3331.
(18) Theis, T.; Truong, M. L.; Coffey, A. M.; Shchepin, R. V.; Waddell, K. W.; Shi, F.; Goodson, B. M.; Warren, W. S.; Chekmenev, E. Y. *J. Am. Chem. Soc.* **2015**, *137*, 1404−1407.
(19) Kadlecek, S.; Emami, K.; Ishii, M.; Rizi, R. *J. Magn. Reson.* **2010**, *205*, 9−13.
(20) Kuhn, L. T.; Bommerich, U.; Bargon, J. *J. Phys. Chem. A* **2006**, *110*, 3521−3526.
(21) Plaumann, M.; Bommerich, U.; Trantzschel, T.; Lego, D.; Dillenberger, S.; Sauer, G.; Bargon, J.; Buntkowsky, G.; Bernarding, J. *Chem.—Eur. J.* **2013**, *19*, 6334−6339.
(22) Joalland, B.; Schmidt, A. B.; Kabir, M. S. H.; Chukanov, N. V.; Kovtunov, K. V.; Koptyug, I. V.; Hennig, J.; Hövener, J.-B.; Chekmenev, E. Y. *Anal. Chem.* **2020**, *92*, 1340−1345.
(23) Goldman, M.; Jóhannesson, H. *C. R. Phys.* **2005**, *6*, 575−581.
(24) Goldman, M.; Jóhannesson, H.; Axelsson, O.; Karlsson, M. *Magn. Reson. Imag.* **2005**, *23*, 153−157.
(25) Reineri, F.; Boi, T.; Aime, S. *Nat. Commun.* **2015**, *6*, 5858.
(26) Bhattacharya, P.; Chekmenev, E. Y.; Perman, W. H.; Harris, K. C.; Lin, A. P.; Norton, V. A.; Tan, C. T.; Ross, B. D.; Weitekamp, D. P. *J. Magn. Reson.* **2007**, *186*, 150−155.
(27) Cavallari, E.; Carrera, C.; Sorge, M.; Bonne, G.; Muchir, A.; Aime, S.; Reineri, F. *Sci. Rep.* **2018**, *8*, 8366.
(28) Burueva, D. B.; Romanov, A. S.; Salnikov, O. G.; Zhivonitko, V. V.; Chen, Y.-W.; Barskiy, D. A.; Chekmenev, E. Y.; Hwang, D. W.; Kovtunov, K. V.; Koptyug, I. V. *J. Phys. Chem. C* **2017**, *121*, 4481−4487.
(29) Ariyasingha, N. M.; Salnikov, O. G.; Kovtunov, K. V.; Kovtunova, L. M.; Bukhtiyarov, V. I.; Goodson, B. M.; Rosen, M. S.; Koptyug, I. V.; Gelovani, J. G.; Chekmenev, E. Y. *J. Phys. Chem. C* **2019**, *18*, 11734−11744.
(30) Gamliel, A.; Allouche-Arnon, H.; Nalbandian, R.; Barzilay, C. M.; Gomori, J. M.; Katz-Brull, R. *Appl. Magn. Reson.* **2010**, *39*, 329−345.
(31) Das, T.; Kweon, S.-C.; Nah, I. W.; Karng, S. W.; Choi, J.-G.; Oh, I.-H. *Cryogenics* **2015**, *69*, 36−43.
(32) Hövener, J.-B.; Chekmenev, E. Y.; Harris, K. C.; Perman, W. H.; Robertson, L. W.; Ross, B. D.; Bhattacharya, P. *Magn. Reson. Mater. Phys., Biol. Med.* **2009**, *22*, 111−121.
(33) Tam, S.; Fajardo, M. E. *Rev. Sci. Instrum.* **1999**, *70*, 1926−1932.
(34) Hövener, J.-B.; Bär, S.; Leupold, J.; Jenne, K.; Leibfritz, D.; Hennig, J.; Duckett, S. B.; von Elverfeldt, D. *NMR Biomed.* **2013**, *26*, 124−131.
(35) Feng, B.; Coffey, A. M.; Colon, R. D.; Chekmenev, E. Y.; Waddell, K. W. *J. Magn. Reson.* **2012**, *214*, 258−262.
(36) Birchall, J. R.; Coffey, A. M.; Goodson, B. M.; Chekmenev, E. Y. *Anal. Chem.* **2020**, *92*, 15280−15284.
(37) Golman, K.; Axelsson, O.; Jóhannesson, H.; Månsson, S.; Olofsson, C.; Petersson, J. S. *Magn. Reson. Med.* **2001**, *46*, 1−5.
(38) Zhivonitko, V. V.; Kovtunov, K. V.; Chapovsky, P. L.; Koptyug, I. V. *Angew. Chem., Int. Ed.* **2013**, *52*, 13251−13255.
(39) Chae, H.; Min, S.; Jeong, H. J.; Namgoong, S. K.; Oh, S.; Kim, K.; Jeong, K. *Anal. Chem.* **2020**, *92*, 10902−10907.
(40) Reineri, F.; Viale, A.; Giovenzana, G.; Santelia, D.; Dastrú, W.; Gobetto, R.; Aime, S. *J. Am. Chem. Soc.* **2008**, *130*, 15047−15053.
(41) Bhattacharya, P.; Chekmenev, E. Y.; Reynolds, W. F.; Wagner, S.; Zacharias, N.; Chan, H. R.; Bünger, R.; Ross, B. D. *NMR Biomed.* **2011**, *24*, 1023−1028.
(42) Salnikov, O. G.; Nikolaou, P.; Ariyasingha, N. M.; Kovtunov, K. V.; Koptyug, I. V.; Chekmenev, E. Y. *Anal. Chem.* **2019**, *91*, 4741−4746.
(43) Salnikov, O. G.; Chukanov, N. V.; Shchepin, R. V.; Manzanera Esteve, I. V.; Kovtunov, K. V.; Koptyug, I. V.; Chekmenev, E. Y. *J. Phys. Chem. C* **2019**, *123*, 12827−12840.
(44) Barskiy, D. A.; Shchepin, R. V.; Coffey, A. M.; Theis, T.; Warren, W. S.; Goodson, B. M.; Chekmenev, E. Y. *J. Am. Chem. Soc.* **2016**, *138*, 8080−8083.
(45) Barskiy, D. A.; Shchepin, R. V.; Tanner, C. P. N.; Colell, J. F. P.; Goodson, B. M.; Theis, T.; Warren, W. S.; Chekmenev, E. Y. *ChemPhysChem* **2017**, *18*, 1493−1498.
(46) Coffey, A. M.; Shchepin, R. V.; Truong, M. L.; Wilkens, K.; Pham, W.; Chekmenev, E. Y. *Anal. Chem.* **2016**, *88*, 8279−8288.
(47) Tom, B. A.; Bhasker, S.; Miyamoto, Y.; Momose, T.; McCall, B. J. *Rev. Sci. Instrum.* **2009**, *80*, 016108.
(48) Hövener, J.-B.; Chekmenev, E. Y.; Harris, K. C.; Perman, W. H.; Tran, T. T.; Ross, B. D.; Bhattacharya, P. *Magn. Reson. Mater. Phys., Biol. Med.* **2009**, *22*, 123−134.
(49) Kadlecek, S.; Vahdat, V.; Nakayama, T.; Ng, D.; Emami, K.; Rizi, R. *NMR Biomed.* **2011**, *24*, 933−942.
(50) Sutherland, L.-M.; Knudson, J. N.; Mocko, M.; Renneke, R. M. *Nucl. Instrum. Methods Phys. Res., Sect. A* **2016**, *810*, 182−185.
(51) Bradshaw, T. W.; Norris, J. O. W. *Rev. Sci. Instrum.* **1987**, *58*, 83−85.
(52) Birchall, J. R.; Kabir, M. S. H.; Salnikov, O. G.; Chukanov, N. V.; Svyatova, A.; Kovtunov, K. V.; Koptyug, I. V.; Gelovani, J. G.; Goodson, B. M.; Pham, W.; Chekmenev, E. Y. *Chem. Commun.* **2020**, *56*, 9098−9101.
(53) Ariyasingha, N. M.; Joalland, B.; Younes, H. R.; Salnikov, O. G.; Chukanov, N. V.; Kovtunov, K. V.; Kovtunova, L. M.; Bukhtiyarov, V. I.; Koptyug, I. V.; Gelovani, J. G.; Chekmenev, E. Y. *Chem.—Eur. J.* **2020**, *26*, 13621−13626.
(54) Salnikov, O. G.; Chukanov, N. V.; Svyatova, A.; Trofimov, I. A.; Kabir, M. S. H.; Gelovani, J. G.; Kovtunov, K. V.; Koptyug, I. V.; Chekmenev, E. Y. *Angew. Chem., Int. Ed.* **2020**, *60*, 2406.
(55) Joalland, B.; Ariyasingha, N. M.; Lehmkuhl, S.; Theis, T.; Appelt, S.; Chekmenev, E. Y. *Angew. Chem., Int. Ed.* **2020**, *132*, 8732−8738.
(56) Appelt, S.; Lehmkuhl, S.; Fleischer, S.; Joalland, B.; Ariyasingha, N. M.; Chekmenev, E. Y.; Theis, T. *J. Magn. Reson.* **2021**, *322*, 106815.
(57) Joalland, B.; Ariyasingha, N. M.; Younes, H. R.; Nantogma, S.; Salnikov, O. G.; Chukanov, N. V.; Kovtunov, K. V.; Koptyug, I. V.; Gelovani, J. G.; Chekmenev, E. Y. *Chem.—Eur. J.* **2020**, DOI: 10.1002/chem.202004168.
(58) Truong, M. L.; Theis, T.; Coffey, A. M.; Shchepin, R. V.; Waddell, K. W.; Shi, F.; Goodson, B. M.; Warren, W. S.; Chekmenev, E. Y. *J. Phys. Chem. C* **2015**, *119*, 8786−8797.
(59) Barskiy, D. A.; Kovtunov, K. V.; Koptyug, I. V.; He, P.; Groome, K. A.; Best, Q. A.; Shi, F.; Goodson, B. M.; Shchepin, R. V.;

Coffey, A. M.; Waddell, K. W.; Chekmenev, E. Y. *J. Am. Chem. Soc.* **2014**, *136*, 3322−3325.
(60) Cowley, M. J.; Adams, R. W.; Atkinson, K. D.; Cockett, M. C. R.; Duckett, S. B.; Green, G. G. R.; Lohman, J. A. B.; Kerssebaum, R.; Kilgour, D.; Mewis, R. E. *J. Am. Chem. Soc.* **2011**, *133*, 6134−6137.
(61) Pravdivtsev, A. N.; Sönnichsen, F. D.; Hövener, J. B. *ChemPhysChem* **2020**, *21*, 667−672.
(62) Kovtunov, K. V.; Kidd, B. E.; Salnikov, O. G.; Bales, L. B.; Gemeinhardt, M. E.; Gesiorski, J.; Shchepin, R. V.; Chekmenev, E. Y.; Goodson, B. M.; Koptyug, I. V. *J. Phys. Chem. C* **2017**, *121*, 25994−25999.
(63) Coffey, A. M.; Kovtunov, K. V.; Barskiy, D. A.; Koptyug, I. V.; Shchepin, R. V.; Waddell, K. W.; He, P.; Groome, K. A.; Best, Q. A.; Shi, F.; Goodson, B. M.; Chekmenev, E. Y. *Anal. Chem.* **2014**, *86*, 9042−9049.

https://dx.doi.org/10.1021/acs.analchem.0c05129
Anal. Chem. 2021, 93, 3594−3601